Morphology, Structure, Rheology, and Thermodynamics of Piezoelectric Poly(vinylidene fluoride)–Ethylene Carbonate Thermoreversible Gel

ARTICLE *in* MACROMOLECULES · DECEMBER 2007

Impact Factor: 5.8 · DOI: 10.1021/ma7021502

7 AUTHORS, INCLUDING:

Ashesh Garai
University of Southampton
20 PUBLICATIONS **546** CITATIONS

SEE PROFILE

Arnab Dawn
Indian Association for the Cultivation of Scie…
26 PUBLICATIONS **601** CITATIONS

SEE PROFILE

Jean-Michel Guenet
University of Strasbourg
174 PUBLICATIONS **2,662** CITATIONS

SEE PROFILE

Morphology, Structure, Rheology, and Thermodynamics of Piezoelectric Poly(vinylidene fluoride)−Ethylene Carbonate Thermoreversible Gel

D. Dasgupta,[†] S. Manna,[†] A. Garai,[†] A. Dawn,[‡] C. Rochas,[§] J. M. Guenet,*[,‡] and A. K. Nandi*[,†]

Polymer Science Unit, Indian Association for the Cultivation of Science, Jadavpur, Kolkata, 700 032, India, Institut Charles Sadron, CNRS UPR 22, 6, Rue Boussingault, 67083 Strasburg, Cedex, France, and Laboratoire de Spectrometrie Physique CNRS-UJF UMR5588, 38402 Saint Martin d'Heres Cedex, France

Received September 26, 2007; Revised Manuscript Received November 17, 2007

ABSTRACT: Poly(vinylidene fluoride) (PVF_2) produces a thermoreversible gel with the important solvent, ethylene carbonate, which is used as a dispersing medium in a lithium ion battery. This is evidenced from the fibrillar network morphology and reversible first-order phase transition of the gels. The invariance of the storage and loss modulus with frequency at lower temperatures (≤110 °C) and the existence of a crossover point between them at higher temperatures further supports thermoreversible gel formation in the system. Solvent subtracted FTIR spectra of the gels indicate formation of a β polymorph, which is retained even after drying using cyclohexane as a guest solvent. The wide-angle x-ray scattering (WAXS) diffractogram of the dried gel also indicates formation of the piezoelectric β polymorph, giving a first time report of thermoreversible piezoelectric gel formation. The temperature−concentration phase diagram in conjunction with Tamman's plot indicates the presence of a polymer−solvent molecular compound whose stoichiometry is around 1.2 solvent molecules/monomer unit. The presence of eutectic and metatectic transitions in the PVF_2− ethylene carbonate (EC) system is also evidenced from the phase diagram. Time-resolved X-ray diffraction patterns also show a new peak at $q = 13.15$ nm^{-1} which is assigned to the molecular compound on the basis of a possible crystalline lattice. Molecular modeling using molecular mechanics calculations with the MMX program supports polymer−solvent complex formation. It also indicates that electrostatic and H-bonding forces are operating side by side on the carbon skeleton fixing the all trans chain conformation of β PVF_2 in the gel.

Introduction

Poly(viny1idene fluoride) (PVF_2) is a technologically important polymer, for its piezoelectric and pyroelectric properties, nonlinear optical susceptibility, and for an unusually high dielectric constant.[1,2] PVF_2 is 50% crystalline and it exists in five different crystalline polymorphs.[1,3] The most common polymorph is α with a monoclinic unit cell and a $TGT\bar{G}$ chain conformation,[4] the piezoelectric β polymorph has an all trans conformation with an orthorhombic unit cell,[5] and the γ phase has an orthorhombic unit cell with a $T_3GT_3\bar{G}$ chain conformation.[6] The δ and ϵ polymorphs are polar and antipolar analogs of the α and γ forms, respectively.[7] Thermoreversible gelation of PVF_2 has received significant attention because of its possible use as a polymer gel actuator (semirigid transducer),[8−12] and in some recent reports, these PVF_2 gels have been shown to produce multiporous materials (pore diameter ranges from a few nanometers to a few hundred micrometers) with a possible use for separation of impurities of various sizes.[13,14] Thus, thermoreversible PVF_2 gels are really interesting for their diverse use in material science. Recently, PVF_2 and its copolymers are used extensively in the lithium ion battery in conjunction with a mixture of ethylene carbonate (EC) and propylene carbonate (PC) together with lithium salts ($LiClO_4$, $LiCoO_2$, etc.).[15−17] However, no report yet exists in the literature about the nature of the thermodynamic interaction between the solvent EC or PC with PVF_2 and whether the solvent has any capability to produce any specific polymorph of PVF_2. To understand the above properties of this important system, we report here a thermodynamic, morphological, structural, and rheological study of this PVF_2−EC system.

PVF_2 produces thermoreversible gels with a bicyclic ketone, camphor, which acts as a solid gelator.[18] The gelation occurs as a result of polymer−solvent compound formation,[19−21] which involves major structural changes of both the components.[18] In this paper, we report the thermoreversible gelation of PVF_2 with the important solvent ethylene carbonate (EC) which is a solid below 37 °C. Ethylene carbonate is extensively used as a nonaqueous electrolyte in lithium-ion batteries, which are presently becoming popular power sources for advanced portable electronics such as notebook computers and cellular phones.[22] In the lithium ion batteries, generally, a mixture of EC and PC are used with PVF_2 and lithium salts. To understand the thermodynamics of the complex system, we begin with the simple PVF_2−EC system. EC has a carbonyl group, which has specific interaction with the $>CF_2$ dipole of PVF_2.[23−25] Consequently, there is also a chance of polymer−solvent complex formation which would like to produce fibrils and may produce a thermoreversible gel.[11,12] In this manuscript, we present the morphology, structure, rheological properties, and temperature−concentration phase diagram of this important system. This knowledge will be extended later on, for the complete understanding of the thermodynamics of the PVF_2 supported lithium ion battery.

* To whom correspondence should be addressed. E-mail: psuakn@mahendra.iacs.res.in (A.K.N.); guenet@ics.u_strasbg.fr (J.M.G.).
† Indian Association for the Cultivation of Science.
‡ Institut Charles Sadron, CNRS UPR 22.
§ Laboratoire de Spectrometrie Physique CNRS-UJF UMR5588.

10.1021/ma7021502 CCC: $40.75
Published on Web 12/29/2007

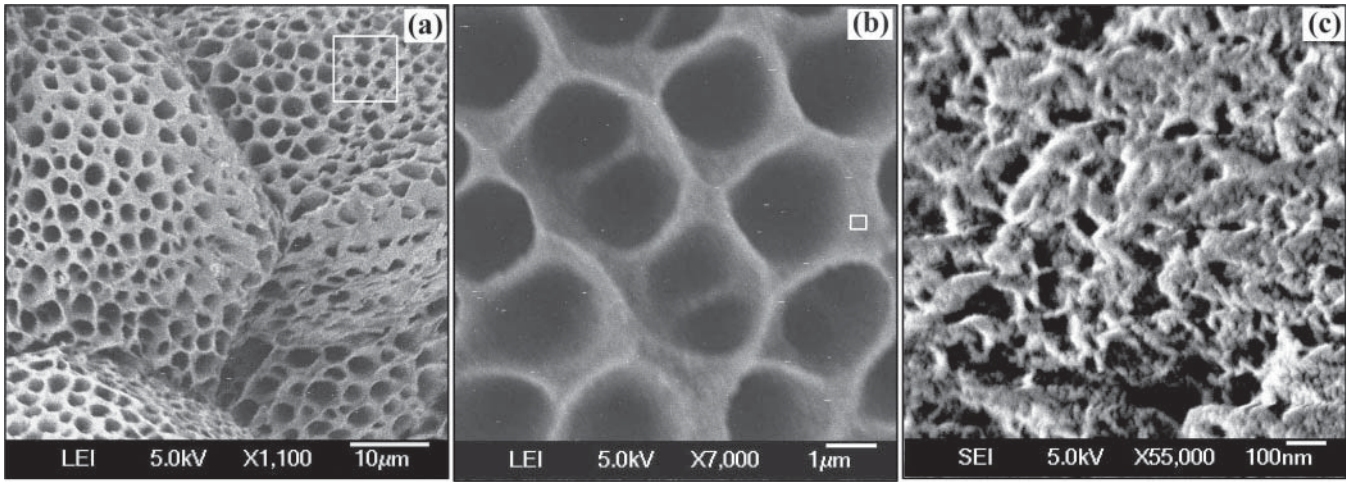

Figure 1. FESEM micrographs of dried PVF_2−EC ($W_{PVF2} = 0.30$) gel at three different magnifications from the indicated square marks.

Experimental Section

Samples. Poly(vinylidene fluoride) (PVF_2) was purchased from Aldrich Chemical Co., Inc. The weight-average molecular weight ($\bar{M}_w$) of the sample is 1.8×10^5, and the polydispersity index is 2.54, as reported from the company. The PVF_2 sample was purified by recrystallization from its 0.2% (w/w) solution in acetophenone. The head to head (H−H) defect of the sample was measured from the ^{19}F NMR spectra of recrystallized PVF_2 in DMF-d_7 using a 300 MHz (Bruker) instrument. The H−H defects were calculated by regrouping seven carbon sequences into five carbon sequences[3] and was found to be 5.09 mol %. Ethylene carbonate was purchased from Sigma-Aldrich Chemical Co. and was used without any further purification.

Sample Preparation. The PVF_2 and EC with appropriate weight fractions were taken in thick walled glass tubes (8 mm in diameter and 1 mm thick) and were sealed. The samples in the sealed tubes were melted at 210 °C in an oven for 20 min with intermittent shaking to make it homogeneous. The shaking was performed in a rotor (Remi, Cyclo-Mixer). The transparent solution was then quenched to 30 °C to form the gel.

Scanning Electron Microscopy. To view the morphology of the PVF_2−EC system, the gels were dried by the solvent replacement method by leaching with a guest solvent, cyclohexane.[13,14] A thin portion of the gel was immersed into cyclohexane, which was replaced by fresh batches at every 12 h interval. This process was continued for 10 days and the film was finally leached by methanol and dried in vacuum at 30 °C for 3 days. The morphology of the above dried gels was recorded in a field emission scanning electron microscope (FESEM) apparatus (JEOL, JSM-6700F). The samples were platinum coated by the sputtering technique in an argon atmosphere and were then observed through the SEM.

Transmission Electron Microscopy. For the TEM study, a thin section of the dried PVF_2−EC gel is prepared by embedding it into an epoxy matrix and cutting in an ultramicrotome (Ultracut R, Leica, Germany) equipped with a glass knife at 25 °C. The thin section (thickness ~70 nm) was then placed on a carbon coated copper grid of 200 mesh size and the morphology was observed through a high-resolution transmission electron microscope (JEOL, 2010 EX). The instrument was operated at an acceleration voltage of 200 kV without staining. A CCD camera was used to record the pictures.

FTIR Spectroscopy. FTIR spectra of the PVF_2−EC complexes as well as those of the pure polymer and solvent were recorded using a Perkin-Elmer FTIR spectrophotometer (model spectrum RX-I) with 2 cm^{-1} resolution. All the spectra were taken in absorbance mode. To get the IR bands arising from the PVF_2 chains in the PVF_2 −EC complexes, the spectrum of pure EC was quantitatively subtracted from that of the complex using the software Spectrum (version 5.0.1). The FTIR spectra of dried gels were also done by making KBr pellets with the dried samples.

Differential Scanning Calorimetry. The thermal behavior of these systems was investigated by means of Diamond DSC [Perkin-Elmer] under an N_2 atmosphere. The weighed amount of the gel sample was determined once placed into hermetically sealed aluminum pans. They were homogenized at 200 °C for 10 min and then quenched to −30 °C and kept at this temperature for 20 min. They were then heated at the scan rate of 10°/min from −30 to 200 °C. Cooling runs were also taken from the melt at 200 to −30 °C at the rate of 5 °C/min. The weight of the sample pan was checked after each experiment, and the instrument was calibrated with cyclohexane and indium before each set of experiments. The thermograms were analyzed, and the corresponding enthalpies were calculated with a personal computer using PYRIS software (version 7.0).

WAXS Investigation. The wide-angle X-ray diffraction experiments of the dried PVF_2−EC gels were performed in a Seifert X-ray diffractometer (C3000) with a nickel filtered copper K_α radiation, equipped with a parallel beam optics attachment. The instrument was operated at a 35 kV voltage and a 30 mA current and was calibrated with a standard silicon sample. The samples were scanned from a $2\theta = 2$ to 37° value at the step scan mode (step size 0.03°, preset time 2 s), and the diffraction pattern was recorded using a scintillation counter detector.

Time-Resolved X-ray Diffraction. The temperature-dependent wide-angle X-ray experiments of PVF_2−ethylene carbonate systems were carried out on beam line BM2 at the European Synchrotron Radiation Facility (ESRF), Grenoble, France. The energy of the beam was 15.8 keV, which corresponds to a wavelength of $\lambda = 7.86 \times 10^{-2}$ nm. The collimated beam was focused with a typical cross section of 0.1×0.3 mm^2. The scattered radiation was collected onto a two-dimensional CCD detector. Data acquisition times were about 10−20 s, which allows collecting data every 3 °C at a heating rate of about 2 °C/min.

The momentum transfer vector q range was $5 < q\ (nm^{-1}) < 18$, with $q = (4\pi/\lambda)\ \sin(\theta/2)$, where λ and θ are the wavelength and the scattering angle, respectively. The scattered intensities were corrected for detector efficiency, dark current, empty cell scattering, sample transmission, and sample thickness. A one-dimensional X-ray pattern was obtained by radially regrouping the data and using a silver behonate sample for calibrating the q-scale. The samples were placed in glass tubes of 3 mm diameter that were sealed to prevent solvent loss. A minimum of 200 mg of material was used in order to make sure that the sample was homogeneous throughout.

Rheological Measurement. Rheological characterization of the PVF_2−EC gels was done using an Advanced Rheometer AR 2000 (TA Instrument). The experiments were performed by using cone and plate geometry on the peltier plate. The cone diameter was 40 mm, cone angle 1° 59′ 56″, and the truncation of the geometry was 56 μm. The PVF_2−EC gel ($W_{PVF2} = 0.30$) was first made in a gelation tube and then it was transferred on the peltier plate to

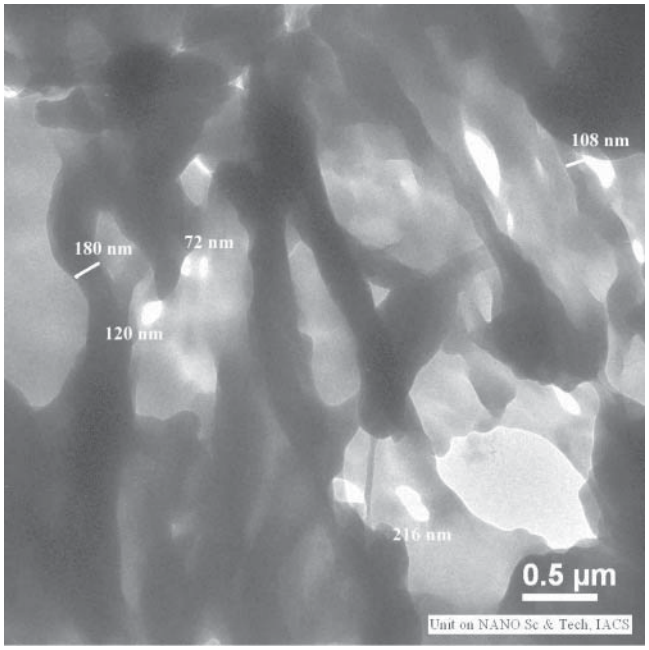

Figure 2. TEM micrograph of dried PVF_2−EC gel of composition $W_{PVF2} = 0.30$. (Pores of different diameters are also marked in the figure.)

remove the air gap with the cone. The sample was loaded at 110 °C and then immediately cooled to 20 °C, where, it was kept for 10 min to equilibrate with the temperature. The temperature sweep experiment was done from 20 to 135 °C at the heating rate of 10°C/min using very low-frequency, e.g., 1 Hz. The frequency sweep experiments were performed in the frequency range between 0.1 and 100 Hz at three different temperatures, namely, 80, 110, and 120 °C. The data obtained were analyzed with the help of "Rheology Advantage Data Analysis" software, version V5.2.19.

Molecular Modeling. An approximate molecular model of the PVF_2−EC complex is obtained from a personal computer (pentium-III) using a molecular mechanics (MMX) program. The zigzag structure of β-polymorph PVF_2 and the structures of ethylene carbonate molecules are drawn with the help of the program such that the oxygen atom of the >C═O group of EC faces the carbon atom of $>CF_2$ group of PVF_2, i.e., the EC molecules are placed between the parallel zigzag chains of PVF_2. The whole structure was then energetically minimized with the help of the MMX program in the computer. The distances between the carbon atom of the $>CF_2$ group and the oxygen atom of the >C═O group, ring oxygen, and H-atom of the $>CH_2$ group are queried and also that between the two PVF_2 strands of the complex from the program.

Results and Discussion

Thermoreversible Gel. In Figure 1, the FESEM pictures of the dried gel of composition $W_{PVF2} = 0.30$ are presented for different magnifications. The lowest magnified picture of the figure clearly shows the porous matrix in the dried gel, and at higher magnification it indicates the presence of honeycomb type pores. On further magnification of the pore walls, smaller dimension fibrils with a significant amount of branching and having smaller size pores are observed. So the dried gel contains pores of both macro and meso dimensions with a fibrillar network morphology. In Figure 2, the TEM micrograph of the microtomed section of the dried gel (dried from the gel of composition $W_{PVF2} = 0.30$) is presented. Here also pores of different diameters (≥70 nm) embedded in the fibrillar network matrix are clearly observed.

In Figure 3, the representative DSC patterns of the PVF_2−EC gel ($W_{PVF2} = 0.42$), for both the heating and cooling processes, are shown. In the heating thermogram, the endothermic peaks are observed at two different temperature regions, the lower temperature peak is due to the melting of EC crystals and the higher temperature peak corresponds to the melting of PVF_2 in the gel state. There are two humps in both parts of the diagrams that will be discussed later. On cooling the melt from 200 °C at the rate of 5 °C/min, two exotherms are obtained as shown in the Figure 3. It is apparent that the higher temperature exothermic peak is due to the gelation of the PVF_2−EC system, while the lower temperature exothermic peak at −23 °C is due to crystallization of the free EC in the gel. Thus, from the DSC thermograms it is evident that the PVF_2−EC system has both fibrillar network morphology and reversible first-order phase transition characterizing the system as a thermoreversible gel.[26,27]

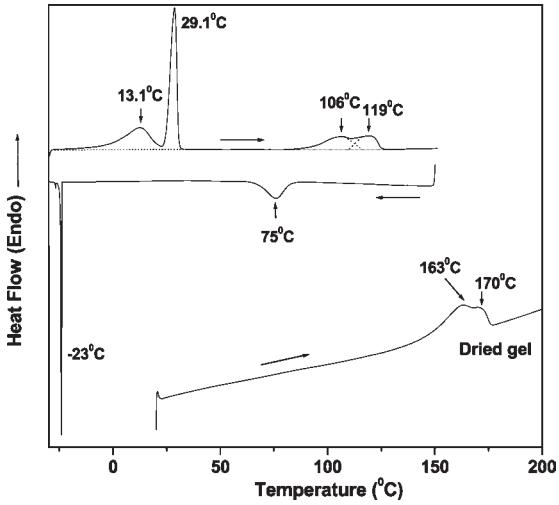

Figure 3. Typical DSC heating and cooling thermograms for PVF_2−EC gels of compositions $W_{PVF2} = 0.42$ and heating thermogram of dried PVF_2 (dried from the gel), taken at the heating rate 10 °C/min and cooling rate 5 °C/min. The dotted lines are drawn to indicate the deconvolution procedure.

A further support of thermoreversible gel formation in the PVF_2−EC system ($W_{PVF2} = 0.30$) has been afforded from the rheological viewpoint. In Figure 4a, the storage modulus of the system is shown at three different temperatures, namely, 80, 110, and 120 °C for the applied frequency range 0.1−100 Hz. It is apparent from the figure that at 80 °C both the storage modulus and loss modulus are parallel to the frequency axis and the storage modulus values are higher than that of the loss modulus characterizing the system in the gel state. At 110 °C, the loss modulus values are higher than the storage modulus at the low-frequency region (≤0.8 Hz), but at the high-frequency region, the storage modulus values are lying above the loss modulus values showing a cross over point. This indicates that the system at 110 °C behaves as a sol for the frequency region below 0.8 Hz and above that frequency it is behaving as a gel. Finally at 120 °C, the system behaves completely as a sol because the loss modulus values are higher than that of the storage modulus values. From a rheological viewpoint, the gel state is described as $G'(\omega) > G''(\omega)$, $G' \sim \omega^0$, $G'' \sim \omega^0$ and the sol state as $G''(\omega) > G'(\omega)$, $G' \sim \omega^2$, $G'' \sim \omega$ at the lower frequency region (0.1−1 Hz).[28,29] In the above logarithmic plots, the slope values corresponding to the storage modulus G′ is 0, 0.45, and 1.94 at temperatures 80, 110, and 120 °C, respectively, while that for G″ is 0.05, 0.17, and 0.80. These results indicate that the system behaves as a gel below 110 °C, and at 120 °C, the gel completely melts to yield a sol state. The above results are also found to be consistent with the DSC results (gel melting peaks 98.8 and 109.3 °C). Thus the rheological study concludes that the PVF_2−EC system produces

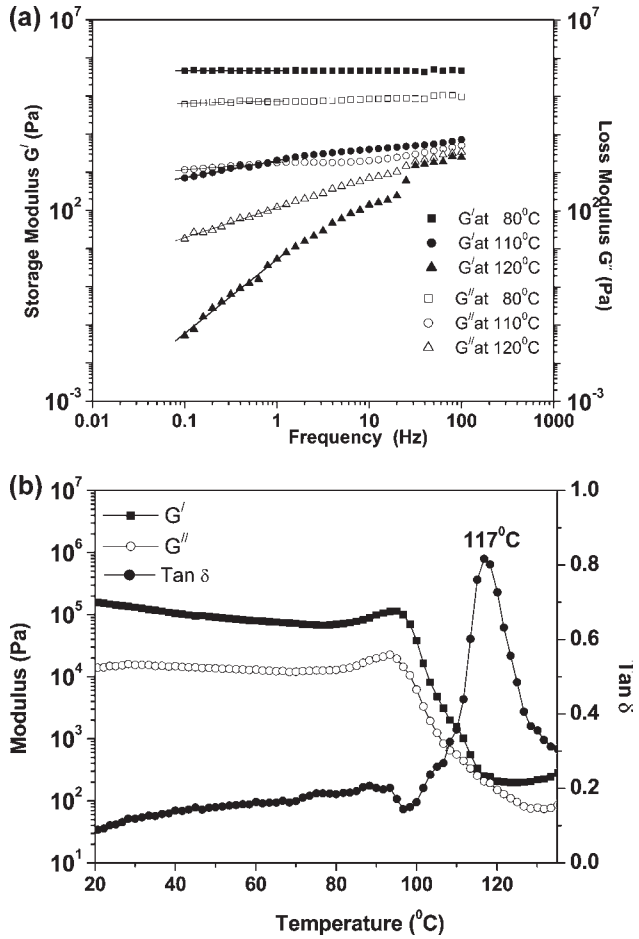

Figure 4. (a) Plot of storage modulus and loss modulus against angular frequency for PVF_2−EC ($W_{PVF2} = 0.30$) gel at the indicated temperatures. The symbols represent the experimental data and the solid lines are the linear fit to determine the slope in the low-frequency region. (b) Plot of storage modulus, loss modulus, and tan δ (measured at 1 Hz frequency) with temperature for the PVF_2−EC ($W_{PVF2} = 0.30$) gel.

a thermoreversible gel. From the temperature ramp experiment, it is evident that at low temperature the system behaves as a thermoreversible gel (Figure 4b), when G′ > G″ up to 110 °C. Around 100 °C, the gel starts melting and at 116.8 °C the G′ and G″ become equal. Tan δ shows a peak at temperature 117 °C, which is equal to the gel melting temperature obtained from equality of G′ and G″.

Structure. The structure of the PVF_2−EC system has been determined from FTIR and a WAXS study. In Figure 5a the solvent subtracted FTIR spectra of the PVF_2−EC gels are presented and it is apparent from the spectra that the PVF_2 has β-polymorphic structure in the gel. The α polymorph is characterized by vibrational bands at 795, 763, 613, and 532 cm^{-1} while the β polymorph has the characteristic peaks at 442, 470, 510, and 840 cm^{-1}.[30,31] The 1283, 840, 508, and 442 cm^{-1} are for the trans zigzag conformation of β polymorph PVF_2. It is clear from the above solvent subtracted spectra of the gel of composition $W_{PVF2} = 0.10$ that the α peaks are completely absent, and the appearance of the peaks at 442, 470, 508, and 840 cm^{-1} confirm the formation of the β polymorph in the gel. This is true for all other compositions, e.g., $W_{PVF2} = 0.20$, 0.30, and 0.38 of the gels indicating the PVF_2−EC system produces gels of β-polymorphic PVF_2. So far gels of β-polymorphic PVF_2 are not reported, and this system is really important as β-polymorph PVF_2 has piezoelectric properties.

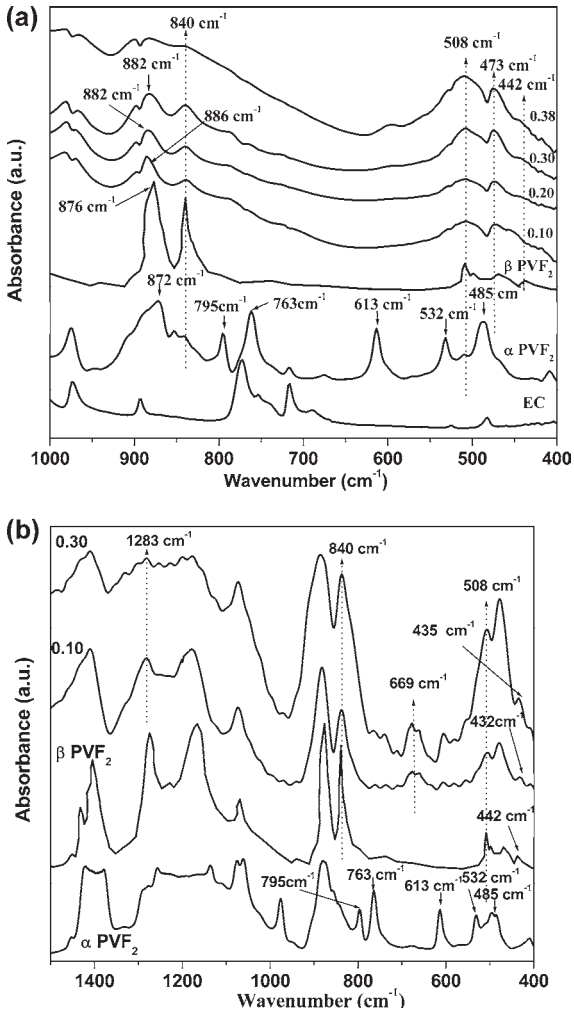

Figure 5. (a) Solvent subtracted FTIR spectra of PVF_2−EC gels for gel compositions $W_{PVF2} = 0.10$, 0.20, 0.30, and 0.38 along with the FTIR spectra of the melt-crystallized PVF_2 and that of EC. **(b)** FTIR spectra of dried PVF_2−EC systems for compositions $W_{PVF2} = 0.10$ and 0.30 along with the FTIR spectra of the melt-crystallized PVF_2. Beta polymorph spectra is taken from ref 31.

In Figure 5b, the FTIR spectra of dried PVF_2−EC gels (dried by leaching with cyclohexane) are presented. Here also the dried gels exhibit only the vibrational bands corresponding to the β polymorph of PVF_2, indicating that no change of the β polymorphic structure occurs during drying of the gels. However, it is important to note that the peak at 508 cm^{-1} of β-PVF_2 is fatter in the gel state (Figure 5a) than that in the dried state (Figure 5b). One possible way to explain the result is that there is interaction between the $>CF_2$ group of PVF_2 and the >C═O group of EC, and on subtraction this peak remains flattened. In the dried system, the absence of solvent indicates no interaction giving a sharp peak for $>CF_2$ bending. The peak appearing at 442 cm^{-1} is for the rocking CF_2 mode[30,32] and is also broadened due to interaction with the >C═O group of EC. In the dried sample this peak shifts to lower energy 435 cm^{-1} indicating rocking of the CF_2 group is easier in the dried state. Thus, FTIR results indicate strong interaction between the $>CF_2$ dipole of PVF_2 and the >C═O group of EC in the gel state. In the spectra of the dried gel, a new peak is observed at ∼669 cm^{-1} which is absent in both the α and β phase. No definite explanation may be given here, and it might be attributed to the polymer−solvent complexation. The 876 cm^{-1} peak is due to the amorphous phase of PVF_2 (symmetric C−C stretch + CF−CH−CF bend)[24] and the subtracted spectra show a blue

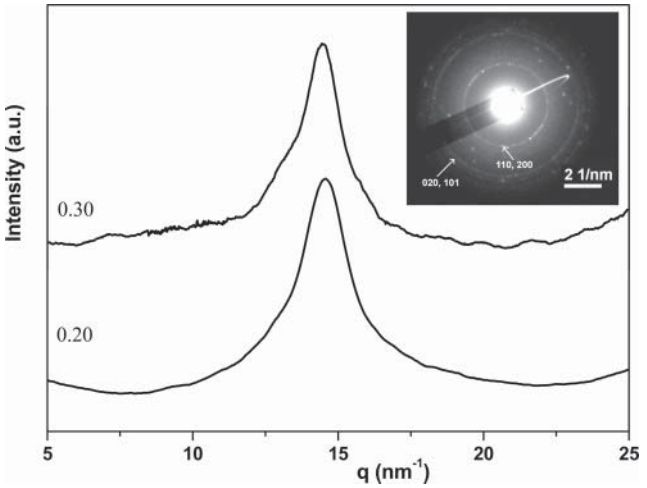

Figure 6. WAXS pattern of the dried PVF_2−EC system dried from the gel composition $W_{PVF2} = 0.20$ and 0.30. (Inset: electron diffraction pattern of fibrils present in Figure 2.)

shift of 6−10 cm^{-1} in the PVF_2−EC systems of different compositions. Probably the polymer−solvent complexation through interaction between $>CF_2$ and $>C{=}O$ dipoles hinders the CF−CH−CF bending vibration causing a shift to higher energy in the spectra. This indicates complexation in the amorphous phase is also occurring.

In Figure 6, the representative WAXS pattern of the dried PVF_2−EC gel with compositions $W_{PVF2} = 0.20$ and 0.30 is presented. It is very much apparent from the figure that there is a single peak at $2\theta = 20.3°$ ($q = 14.57$ nm^{-1}) which corresponds to the pure β polymorph of PVF_2.[4,5] The same conclusion may be extended to that in the gel state as there is no change of polymorphic structure during drying as evident from FTIR results discussed above. In the inset of the Figure 6, the electron diffraction pattern of the fibrils in the micrograph of Figure 2 is presented. Here two diffraction rings characterizing d_{hkl} values of the β polymorph of PVF_2 at 4.41 and 2.56 Å are present. This indicates the β crystallites of the fibrils are polycrystalline in nature. The crystalline thickness of the crystallites measured from WAXS patterns using the Scherrer equation are 4.23 and 3.32 nm for gels of composition $W_{PVF2} = 0.2$ and 0.3, respectively.

Temperature−Concentration Phase Diagrams. Typical DSC thermograms are drawn in Figure 3. Two distinct events can be observed.

As discussed above, the low-temperature endotherm corresponds to the melting of the solvent. For the pure solvent this endotherm consists of only one peak, whereas for concentrated systems a second, broad peak is seen. This is a classical effect due to the porous morphology of the gel. Finite-size crystals of solvent molecules are formed in these pores, whose size is decreasing with polymer concentration while their fraction increases. The melting temperature of these crystals is then significantly lower than that of the infinite crystals on account of the non-negligible surface free-energy. For mapping out the temperature−concentration phase diagram, the melting enthalpy of the solvent is, however, determined from the total area of the solvent melting endotherm as this latent heat is not size-dependent. This enthalpy corresponds to the "free" solvent, namely, the solvent which is not engaged in the compound or in the solid solution structures.

The high-melting endotherm consists of two peaks in the whole concentration range up to pure PVF_2. This endotherm is therefore deconvoluted as shown in Figure 3 in order to measure

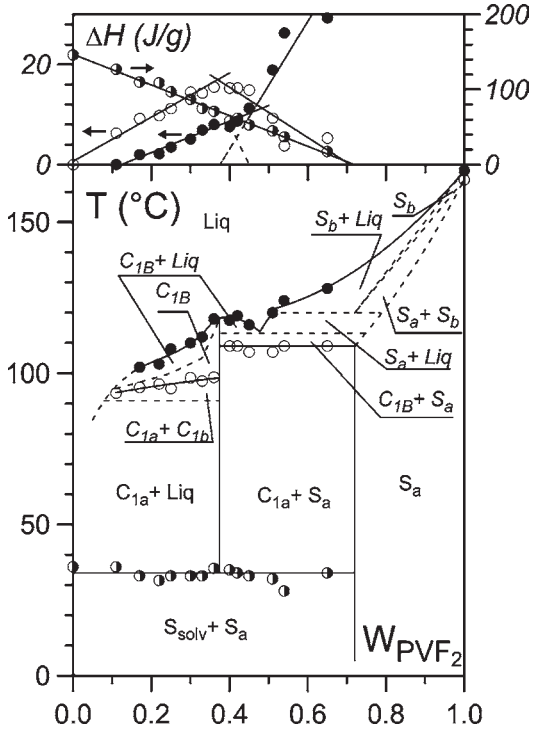

Figure 7. Temperature−concentration phase diagram and Tamman's diagram (ΔH vs concentration) for PVF_2−ethylene carbonate systems. In the Tamman's diagram, the solvent melting enthalpy is given by the right ordinate, while the latent heats associated with the polymer are given on the left ordinate. ◑ = solvent melting temperature; ○ = low-melting temperature; ● = high-melting temperature. C_{1a} and C_{1b} are molecular compounds while S_{sol}, S_a, and S_b are solid phases. As is customary, the transitions deduced from Gibbs phase rules, and the corresponding domains, are shown by means of dotted lines.

the enthalpies associated with each peak. The corresponding temperatures are taken at the maximum of the peaks. As was discussed in our earlier work,[25] this double melting is not due to a melting−recrystallization phenomenon as the ratio between the two endotherms is independent of the heating rate. In fact, two types of lamellae are dealt with, hence the double melting. When a binary system is studied, such as polymer + solvent, this gives rise to a so-called metatectic transition (for details see ref 34). The phase diagram can, therefore, be mapped out by using the procedure that would be applied for a metatectic transformation. Of course, as these lamellae have the same molecular structure, this transition should rather be designated as a "pseudo-metatectic" transformation. The temperature−concentration phase diagram together with its corresponding Tamman's diagram is shown in Figure 7. As can be seen from the Tamman's diagram, the first peak of the high-melting endotherm exhibits a maximum for a polymer concentration of $W_{PVF2} = 0.38$ w/w. This suggests the occurrence of a PVF_2−ethylene carbonate molecular compound with a "thermodynamic" stoichiometry of about 1.2 solvent molecule/monomer unit. Note that this "thermodynamic" stoichiometry may differ significantly from the crystallographic stoichiometry, namely, the number of solvent molecules in the crystal unit cell. As has been shown by Malik et al.,[33] if the degree of crystallinity is low and if the number of solvent molecules per monomer unit in the amorphous domains is higher than in the crystal, then the "thermodynamic" stoichiometry derived from the Tamman's diagram is systematically larger than that of the crystal.

As to the second peak, the associated enthalpies drawn in the Tamman's diagram of Figure 7 display two types of linear behavior. The slope of the linear variation is steeper for $W_{PVF2}>$

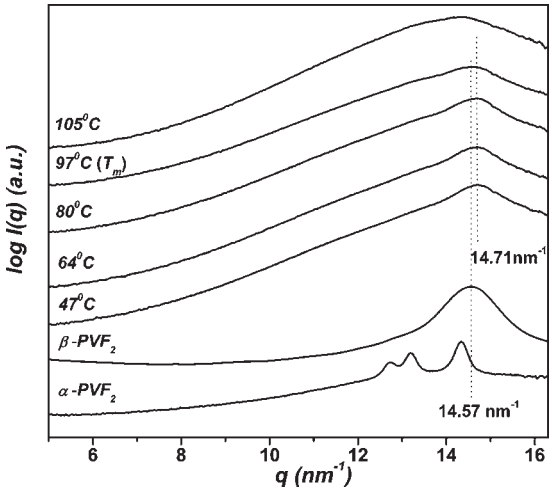

Figure 8. Time-resolved diffraction pattern obtained at a heating rate of about 2 °C/min for $W_{PVF2} = 0.1$. Temperatures are indicated. The diffraction pattern of PVF_2 under the α form and under the β form are also given. Reflections of interest are indicated with vertical lines.

0.45 w/w than that for $W_{PVF2} < 0.45$ w/w. For $W_{PVF2} < 0.38$ w/w, the linear behavior most probably results from the melting of compound C_{1b} which possesses a stoichiometry identical or nearly identical to compound C_{1a}, and whose existence arises from the "pseudo transformation" of C_{1a} into C_{1b} through a pseudo-metatectic process (the first peak of the high melting endotherm). The dotted lines then delimit the possible domains on the basis of this transformation in order to fulfill Gibbs phase rules. Above $W_{PVF2} = 0.38$ w/w, compound C_{1b} forms an eutectic with a solid solution S_a. The term solid solution simply means that solvent can only be occluded in the interlamellar amorphous domains as opposed to the compound where the solvent is located both within the crystalline lattice and the amorphous domains. Again, considering a metatectic transition leads one to deduce the domains drawn in the phase diagram of Figure 7. As a result, the melting behavior above $W_{PVF2} = 0.38$ w/w is mainly that of the solid-phase S_a, hence the drastic change of slope. As will be seen below, the molecular structure of compounds C_{1a} and C_{1b} is related to the β form in the sense that the PVF_2 chains adopt an all-trans conformation. This probably arises from the stabilization of the chain conformation in the compound by the solvent molecules. Conversely, the crystalline domains of S_a are likely to possess the crystal structure of the α form of PVF_2.

Note that the molecular structures can drastically differ whether one quenches a homogeneous solution prepared at high temperature or one uses a drying procedure starting from a low-concentrated system. This is the reason why the β form can be obtained by drying a gel sample whereas the α form grows when quenching from concentrated, homogeneous solutions. Actually, the dried system is not strictly speaking at "equilibrium".

In the concentration range $W_{PVF2} = 0.38$ to 0.45 w/w, the variation of the enthalpies is likely to correspond to the combination of the two linear types of behavior as highlighted by those dotted lines drawn in the Tamman's diagram of Figure 7. At higher concentration, another solid-phase S_b appears again due to the metatectic transformation of S_a, of the same composition and the same molecular structure. Note that the occurrence of a compound of differing composition might have been also contemplated for $W_{PVF2} > 0.45$ w/w. Yet, extrapolation of the enthalpies' linear variation from this concentration range gives a value close to that of the pure α form of PVF_2 so that the existence of a compound of a lower degree of solvation than C_{1a}, and/or C_{1b}, should be discarded.

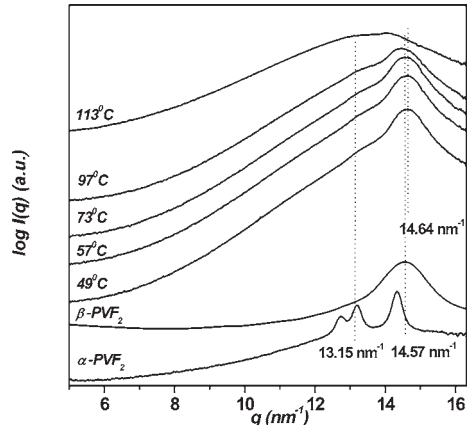

Figure 9. Time-resolved diffraction pattern obtained at a heating rate of about 2 °C/min for $W_{PVF2} = 0.25$. Temperatures are indicated. The diffraction pattern of PVF_2 under the α form and under the β form are also given. Reflections of interest are indicated with vertical lines.

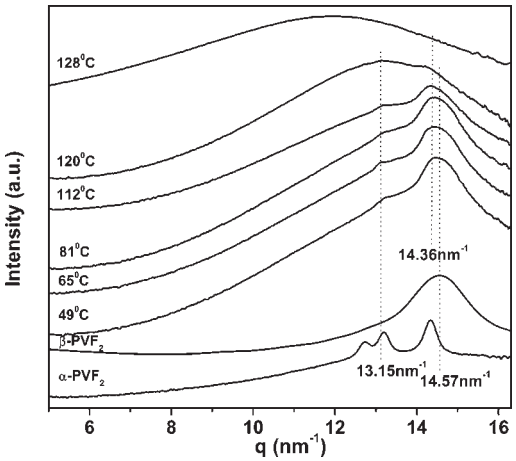

Figure 10. Time-resolved diffraction pattern obtained at a heating rate of about 2 °C/min for $W_{PVF2} = 0.38$. Temperatures are indicated. The diffraction pattern of PVF_2 under the α form and under the β form are also given. Reflections of interest are indicated with vertical lines.

The variation with polymer concentration of the melting enthalpy of the crystallized solvent reveals that beyond $W_{PVF2} = 0.7$, no free solvent molecules are present but that there is still a significant amount of solvent trapped in the polymer-rich phase (otherwise $W_{PVF2} \approx 1$). The fact that this concentration does not match with the maximum of the polymer compound melting enthalpies does not allow one to contemplate the existence of another compound less solvated than compounds C_{1a} and C_{1b}, as already discussed in the above paragraph. The trapped solvent molecules are therefore most probably located in the amorphous domains so that the occurrence of a solid phase should rather be considered. This entails that the following reaction occurs while cooling below the solvent crystallization temperature:

$$C_{1a} + S_a \rightleftharpoons S_{solv} + S_a$$

The transformation of the compound into a solid solution means that the solvent is expelled from the crystal lattice of the compound. This has already been observed in other systems, such as syndiotactic polystyrene/benzene,[35] and results from the fact that the solvent is not tightly bound to the polymer in the compound.

X-ray Diffraction. Typical diffraction patterns obtained by time-resolved X-ray measurements on different PVF_2−ethylene

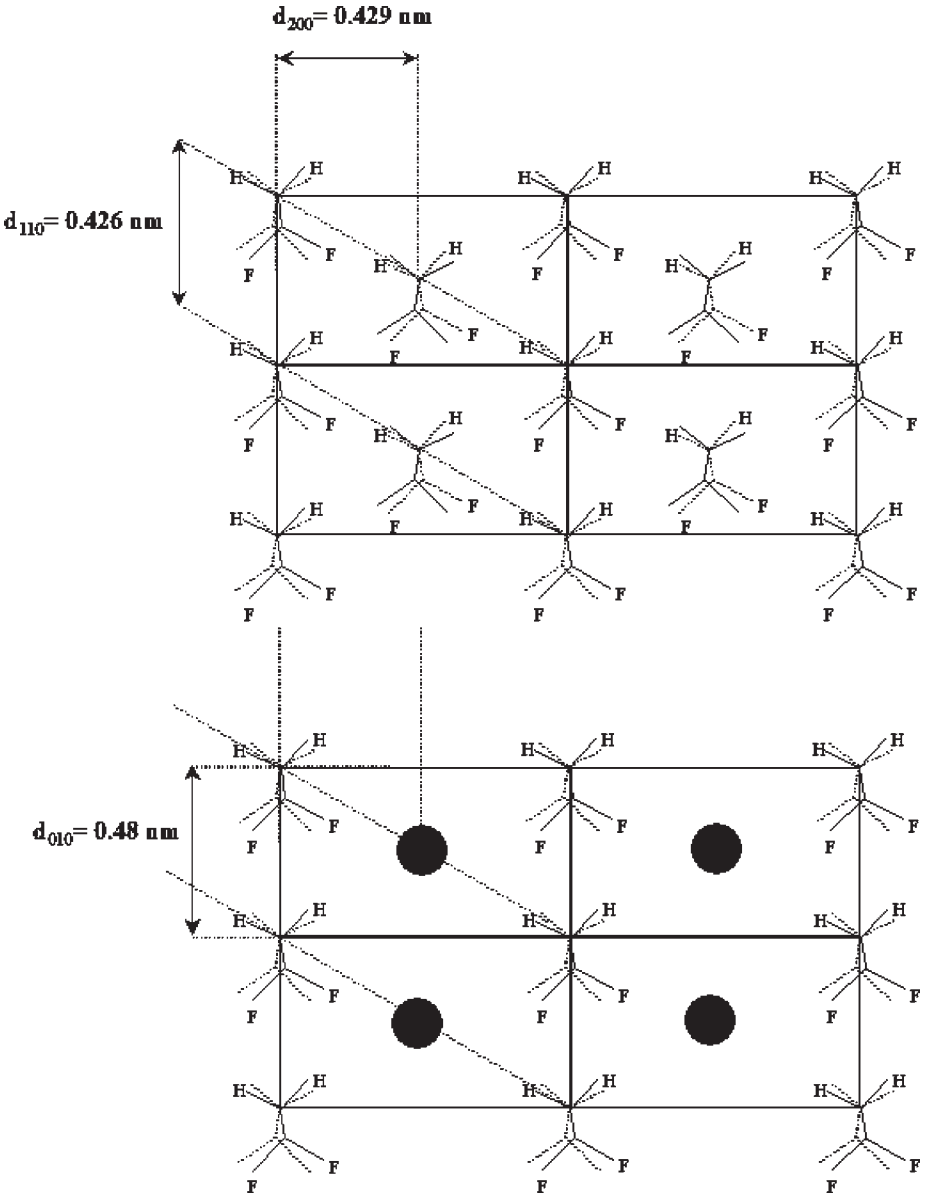

Figure 11. Top: 3 crystalline unit cells of the β form of PVF_2 as seen parallel to the chain axis. Planes giving rise to the peak at $q = 14.64$ nm^{-1} (110) and $q = 14.71$ nm^{-1} (200) are shown. Bottom: a possible model for the solvent intercalation (black dots) in the 110 direction of the crystalline lattice of the β form. The 010 plane that is possibly at the origin of the reflection at $q = 13.15$ nm^{-1} is shown.

carbonate systems are drawn in Figures 8−10. There are two salient features: (i) the patterns differ considerably from that of the α form but only slightly from that of the pure β form PVF_2 and (ii) a peak appears gradually at $q = 13.15$ nm^{-1} which becomes most prominent at $W_{PVF2} = 0.38$, which stands for the stoichiometric composition of the compound as derived from the phase diagram.

The peak at $q = 13.15$ nm^{-1} is certainly not due to the appearance of the α form at high polymer concentrations. Indeed, if it were the case, other peaks should also be observed, particularly at $q = 12.67$ nm^{-1} corresponding to the crystallographic plane 100 of this form ($d_{100} = 0.496$ nm). This clearly suggests that the reflection at $q = 13.15$ nm^{-1} is related to the crystal arrangement of the PVF_2−ethylene carbonate molecular compound.

A possible lattice model is drawn in Figure 11 in an attempt to account for the diffraction pattern. This model is basically built by intercalating solvent molecules in the 110 direction of the original crystalline lattice of the β form. The crystalline unit cell of the β form is considered rather than that of the α form because the drying procedure produces the former not the latter. The reflection at $q = 13.15$ nm^{-1} would then correspond to the 010 plane of the considered lattice while reflections at $q = 14.64$ nm^{-1} and $q = 14.71$ nm^{-1} related to the 110 and 200 planes would still be observed. To be sure, we cannot speculate further with the available data. Additional investigations will be needed to provide support to this model or to put forward another crystalline structure.

Molecular Modeling. An approximate molecular model of the PVF_2−EC compound formation with a single solvent layer within the PVF_2 strands is built up from molecular mechanics calculations using the MMX program[36] (Figure 12). Here, EC molecules are placed on the side of the zigzag β-PVF_2 chain in a way that the carbonyl group of EC faces each $>CF_2$ group of PVF_2 as there is specific interaction between the two.[23,24] Two such solvated PVF_2 chains and a pure PVF_2 chain (to guard the solvent molecules) are taken together and the whole system was energetically minimized through the program. The distances

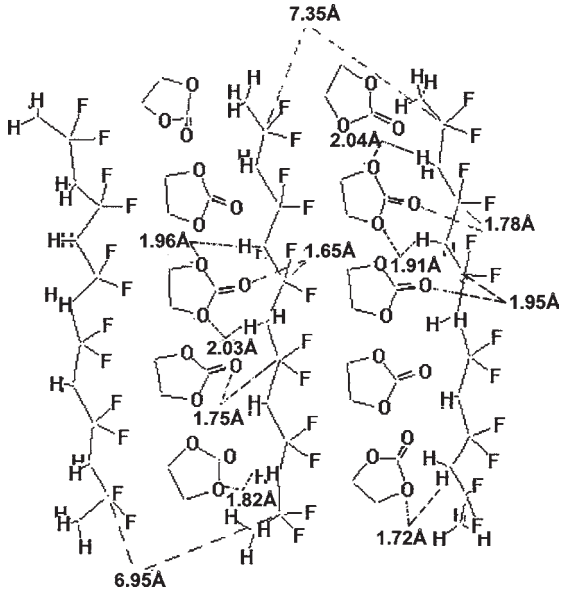

Figure 12. Approximate molecular model of the PVF_2 (β-polymorph)−EC complex obtained from energy minimization through the MMX program.

between the carbon atom of the $>CF_2$ group and oxygen atom of >C═O group are queried and have values in the range 1.78, 1.65, 1.75, 1.95 Å, etc. The van der Waals radii of the $>CF_2$ group is 2.25 Å and that of oxygen is 1.40 Å yielding a distance of interatomic contact of 3.65 Å.[12,37] Here the queried values are much less than 3.65 Å, inferring the PVF_2−EC complex formation is through the dipolar interaction of the $>CF_2$ and >C═O groups in the system. One important point is to note that the distance between the ring oxygen and the hydrogen atom of the CH_2 group is found to be 1.72, 1.82, 1.96, and 2.03 Å which are lesser than the sum of the van der Waals radii of the oxygen (1.40 Å) and hydrogen atoms (1.20 Å).[37] This indicates that weak H-bond formation between the ring oxygen and hydrogen atoms of the $>CH_2$ group might be occurring here. Such H-bond formation between the C−H hydrogen of the polymer chain and the oxygen atom is recently reported by some workers.[38,39] A support for this H-bond formation might be obtained from the solvent subtracted FTIR spectra presented in Figure 13 where a shift of the C−H stretching peak (3024 cm^{-1}) of β-PVF_2 toward a lower wavenumber by 16 cm^{-1} is observed in both the gels. This indicates that in the gel state, electrostatic and H-bonding forces are operating side by side on the carbon skeleton, fixing the conformation of the PVF_2 chain in a zigzag manner. It is probably the reason for the β-polymorph formation than the lower energy α-polymorph formation[40,41] in the PVF_2−EC gel. The average distance between the PVF_2 strands in the model is 7.15 Å indicating microporous material may be prepared by successful removal of EC molecules keeping the gel system intact. At the same time, macropores of large dimension can also be prepared (cf. FESEM micrograph of Figure 1) by proper drying and may yield piezoelectric multiporous polymeric materials.[13,14]

Conclusion

It may be concluded from the above study that PVF_2 produces a thermoreversible gel with the important solvent, ethylene carbonate, as evidenced from fibrillar network morphology and reversible first-order phase transition. Further support of gel formation is obtained from the invariance of the storage and loss moduli at lower temperature (≤110 °C) with frequency, and at higher temperature, a crossover point exists between them indicating the gel melting. Solvent subtracted FTIR spectra of the gels indicate formation of piezoelectric β polymorph, which is retained even in drying using cyclohexane as a guest solvent. Probably this is a first-time report for the formation of a piezoelectric polymeric gel. The temperature concentration phase diagram is very interesting indicating the presence of polymer−solvent complex formation at $W_{PVF2} = 0.38$. The presence of eutectic and metatectic transitions is also evident from the phase diagram. The synchrotron X-ray diffractograms also show a new peak at $q = 13.15$ nm^{-1} probably for the polymer−solvent complex formation. Molecular modeling using molecular mechanics calculations with the MMX program also supports polymer−solvent complex formation. This also indicates electrostatic and H-bonding forces are operating side-by-side on the carbon skeleton, fixing the conformation of the PVF_2 chain in a zigzag manner of β-PVF_2.

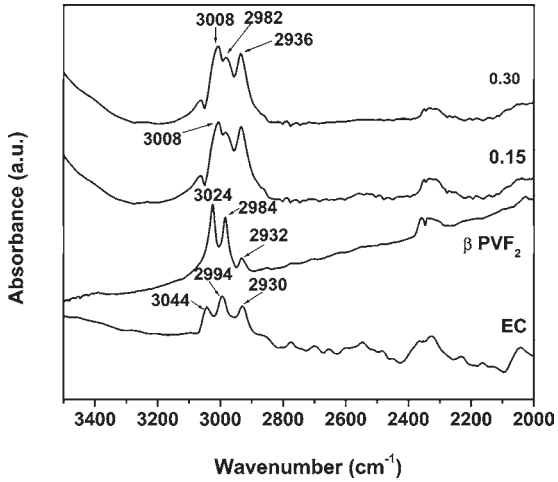

Figure 13. Comparison of C−H stretching frequency from the solvent subtracted FTIR spectra of the PVF_2−EC gel at compositions $W_{PVF2} = 0.15$ and 0.30 with that of the FTIR spectra of pure β-PVF_2.

Acknowledgment. We gratefully acknowledge IFCPAR Grant No. 2808-2 for financial support under the excellent category. We also acknowledge Dr. B. Mukhopadhyay, Central Drug Research Institue, Lucknow, for helping in ^{19}F NMR spectral measurement.

References and Notes

(1) Lovinger, A. J. In *Development in Crystalline Polymers-1*; Basset, D. C., Ed.; Elsevier Applied Science: London, U.K., 1981; p195.
(2) (a) Wang, T. T.; Herbert, J. M.; Glass, A. M. *The Applications of Ferroelectric Polymers*; Blackie: London, U.K., 1988. (b) Xue, G.; Wang, Y.; Liu, S. *Macromolecules* **1995**, *28*, 3476.
(3) Nandi, A. K.; Mandelkern, L. *J. Polym. Sci., Part B: Polym. Phys.* **1991**, *29, 1287.*
(4) (a) Doll, W. W.; Lando, J. B. J. *Macromol. Sci. Phys*. **1970**, *B-4*, 309. (b) Hasagawa, R.; Takahashi, Y.; Chatani, Y.; Tadokoro, H. *Polym. J. (Tokyo)* **1972**, *3*, 600.
(5) (a) Lando, J. B.; Olf, H. G.; Peterlin, A. *J. Polym. Sci., Polym. Chem. Ed.* **1969**, *4*, 941. (b) Galperin Y. L.; Strogalin, Y. V.; Mlenik, M.-P. *Vysokomol. Soedin.* **1965**, *7*, 933.
(6) Weinhold, S.; Litt, M.-M.; Lando, J. B. *J. Polym. Sci.* **1977**, *B-17, 585.*
(7) (a) Davis, G. T.; Mckinney, J. H.; Broadhurst, M. G.; Roth, S. C. *J. Appl. Phys.* **1978**, *49,* 4998. (b) Naegele, D.; Yoon, D. Y.; Broadhurst, M. G.; *Macromolecules* **1978**, *11*, 1297.
(8) Cho, J. W.; Song, H. Y.; Kim, S. Y. *Polymer* **1993**, *34*, 1024.
(9) Mal, S.; Maiti, P.; Nandi, A. K. *Macromolecules* **1995**, *28*, 2371.
(10) Cho, J. W.; Lee, G. W. *J. Polym. Sci.* **1996**, *B34*, 1605.
(11) Dikshit, A. K.; Nandi, A. K. *Macromolecules* **1998**, *31*, 8886.

(12) Dikshit, A. K.; Nandi, A. K. *Macromolecules* **2000**, *33*, 2616.
(13) Dasgupta, D.; Nandi, A. K. *Macromolecules* **2005**, *38*, 6504.
(14) Dasgupta, D.; Nandi, A. K. *Macromolecules* **2007**, *40*, 2008.
(15) Rajendran, S.; Sivakumar, P.; Babu, R. S. *Bull. Mater. Sci.* **2006**, *29*, 673.
(16) Yong-Jun, H.; Bai-Jhen, C.; Yan, Y. *J. Cent. South Univ. (Sci. Technol.)* **2007**, *14* (1), 47
(17) Periasamy, P.; Tatsumi, K.; Shikano, M.; Fujieda, T.; Sakai, T.; Saito, Y.; Mizuhata, M.; Kajinami, A.; Deki, S. *Solid State Ionics* **1999**, *126*, 285.
(18) Dasgupta, D.; Manna, S.; Malik, S.; Rochas, C.; Guenet, J. M.; Nandi, A. K. *Macromolecules* **2005**, *38*, 5602.
(19) Guenet, J. M. *Macromolecules* **1987**, *20*, 2874.
(20) Guenet, J. M.; McKenna, G. B. *Macromolecules* **1988**, *21*, 1752.
(21) Guenet, J. M. *Thermochim. Acta* **1996**, *284*, 67.
(22) Wang, Y.; Balbuene, P. B. *J. Phys. Chem. B* **2002**, 106, 4486.
(23) Roerdink, E.; Challa, G. *Polymer* **1980**, *21*, 509.
(24) Belke, R. E.; Cabasso, I. *Polymer* **1988**, *29*, 1831.
(25) Dasgupta, D.; Malik, S.; Rochas, C.; Thierry, A.; Guenet, J. M.; Nandi, A. K. *Macromolecules* **2006**, *39*, 6110.
(26) Guenet, J. M. *Thermoreversible Gelation of Polymers and Biopolymers*; Academic Press: New York, 1992.
(27) Daniel, C.; Dammer, C.; Guenet, J. M. *Polymer* **1994**, *35*, 4243.
(28) Tiitu, M.; Hiekkataipale, P.; Hartikainen, J.; Makela, T.; Ikkala, O. *Macromolecules* **2002**, *35*, 5212.
(29) te Nijenhuis, K. *Adv. Polym. Sci.* **1997**, *130*, 1.
(30) Kobayashi, M.; Tashiro, K.; Tadokaro, H. *Macromolecules* **1975**, *8*, 158.
(31) Tashiro, K.; Kobayashi, M. *Phase Transitions* **1989**, *18*, 213.
(32) Cortill, G.; Zebri, G. *Spectrochim. Acta* **1967**, *23A*, 2218.
(33) Malik, S.; Rochas, C.; Guenet, J. M. *Macromolecules* **2006**, *39*, 1000.
(34) Guenet J.M. *Polymer-Solvent Molecular Compounds*; Elsevier: Amsterdam, The Netherlands, 2008.
(35) Daniel, C.; De Luca, M. C.; Brulet, A.; Menelle, A.; Guenet, J. M. *Polymer* **1996**, *37*, 1273
(36) Gajewski, K. E.; Gilberr M. H. In *Advances in Molecular Modelling*; Liotta, D., Ed.; JAI Press: Greenerick, CT, 1990; Vol. 2.
(37) Pauling, L. *The Nature of the Chemical Bond and the Structure of Molecules and Crystals: An Introduction to Modern Structural Chemistry,* 3rd ed.; Cornell University Press: Ithaca, NY, 1960; p 227.
(38) Bodige, S. G.; Rogers, R. D.; Blackstock, S. C. *Chem. Commun.* **1997**, 1669.
(39) Hu, Y.; Zhang, J.; Sato, H.; Futami, Y.; Noda, I.; Ozaki, Y. *Macromolecules* **2006**, *39*, 3841.
(40) Farmer, B. L.; Hopfinger, A. J.; Lando, J. B. *J. Appl. Phys.* **1972**, *43*, 4293.
(41) Datta. J.; Nandi, A. K. *Polymer* **1997**, *38*, 2719.

MA7021502